LANGMUIR

Interfaces: Adsorption, Reactions, Films, Forces, Measurement Techniques, Charge Transfer, Electrochemistry, Electrocatalysis, Energy Production and Storage

Drop capturing based on patterned substrate in space

Weibin Li, Ding Lan, Honghui Sun, and Yuren Wang

Langmuir, **Just Accepted Manuscript** • DOI: 10.1021/acs.langmuir.8b00219 • Publication Date (Web): 28 Mar 2018

Drop capturing based on patterned substrate in space

Weibin Li, Ding Lan,* Honghui Sun, Yuren Wang†

National Microgravity Laboratory, Institute of Mechanics, Chinese Academy of Sciences, 100190 Beijing, China

and School of Engineering Sciences, University of Chinese Academy of Sciences, 100049 Beijing, China

E-mail: *landing@imech.ac.cn; †yurenwang@imech.ac.cn.

ABSTRACT

In this work, we introduced a method for capturing aqueous drop based on a patterned substrate in space. Through the manipulation test of a colloidal drop, it could be verified that this patterned substrate had excellent control ability for aqueous drop in microgravity condition. The confinement mechanism of this substrate was clarified, which showed that drops with different volume could be pinned and attracted at a given area on the substrate. The confinement capability was related to the gravity effect, and the patterned substrate could confine aqueous drops with larger volume under microgravity than in normal gravity. With advantages of simple operation and strong capability to control large drops, this technique exhibited the wide application prospect in the fields of fluid management, bio-sensing, pharmacy in microgravity condition in the future.

Key words: Microgravity; drop manipulation; patterned substrate; contact angle; evaporation

I. INTRODUCTION

The manipulation of liquid drops under microgravity environment could be very promising in space applications, such as life support systems, waste water treatment, heat exchangers, machining biologics and pharmacy.[1-3] Over the past two decades, a variety of microgravity experiments concerning growth and manipulation of liquid drops had been performed. Antar et al. performed drop coalescence experiments through two hypodermic needles which were contacted using manual force, allowing the drops to coalesce[4]. Savino et al. examined wetting and coalescence of silicone oil sessile drops formed over copper substrates using a cylindrical copper needle with a coaxial hole[5]. To investigate gravity effect on the contact angle and the drop interface shape, Brutin et al. created drops by injection through a hole of the substrate[6]. All these works had already led to major advances for the drop manipulation in space. However, these solutions were too complicated, furthermore, the drops couldn't be fully constrained, which was likely to be unstable under vibration or attitude adjustment of the spacecraft. A more simple and reliable technique was necessary for the control of liquid drops under the conditions of weightlessness.

Patterned substrates on the basis of wetting enhancement or wetting barrier were always designed to manipulate the drop in terrestrial condition.[7-12] For examples, Lai and co-workers reported a super-hydrophobic/hydrophilic patterned surface with photocatalytic TiO_2 nanotubes.[13] Tenjimbayashi et al. introduced a liquid manipulation strategy to design dynamically hydrophobic and statically hydrophobic/hydrophilic patterned surfaces.[14] Dong and McCarthy described a method for preparing super-hydrophobic surfaces containing

guiding lines that control water motion.[15] Draper et al. designed the patterned surface with a super-hydrophobic polymer coating for the manipulation of droplets within microfluidic channels.[16] Zhang et al. designed super-hydrophobic TiO_2 nanostructures for condensate micro-drop self-propelling.[17] Wu et al. designed Laplace pressure pattern based on conical morphology and wetting heterogeneity for microdroplet manipulation.[18]These works illustrated that the patterning technology had excellent performance in drop manipulation under terrestrial condition. We might wonder whether it was feasible to expand this technology to space as well. In fact, the drops could be easily kept stable on a substrate under the gravity force on earth that has nothing to do with the surface modification of the substrate. However, in microgravity environment, gravitational effects were negligibly small and surface tension effects dominated the liquid behavior,[19] thus the liquid can climb along the wetting surface[20-21], which might be easily to result in catastrophic effects in space. Therefore, the applicability of drop manipulation through modifying the surface wettability in microgravity environment was still a problem that await for proof.

In this work, we performed microgravity experiments of drop manipulation on the SJ-10 satellite,[22] and succeeded in realizing the drop capturing based on a patterned substrate. We had further analyzed the confinement mechanism of the substrate by drop evaporation. In addition, the gravity effect on the confinement capability of the patterned substrate was illustrated through theoretical and experimental studies.

II. EXPERIMENTAL METHODS

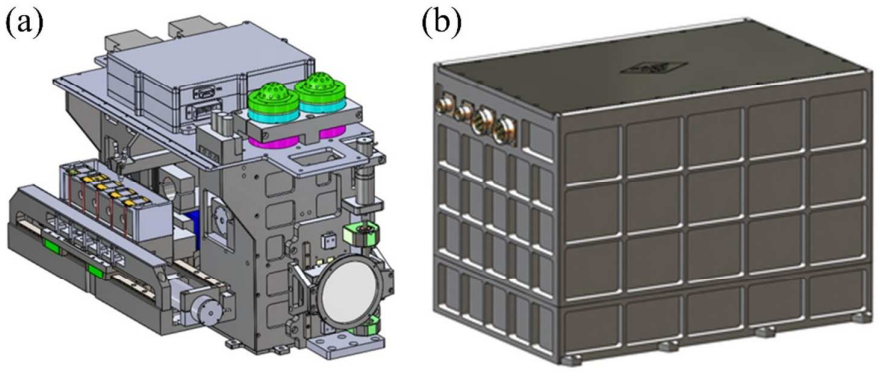

Figure 1. The experimental setup of the colloidal material box (CMB) in the SJ-10 satellite. (a) the internal structure and (b) the appearance of the CMB.

Colloidal Material Box. The SJ-10 satellite was specifically designed for scientific research, which provided a mission of space experiments including both fields of microgravity science and space life science. The SJ-10 satellite was started by the Chinese Academy of Sciences (CAS) and launched in April 2016.[22] The colloidal material box (CMB) (see Figure 1), as one of several experimental boxes aboard the SJ-10 satellite, was proposed to study the complex fluids physics in microgravity, including the colloidal assembling dynamics of an evaporative droplet and liquid crystal phase transition in space.[23] The satellite had been stayed 18 days and created sustained and favorable microgravity environment (10^{-4}g).

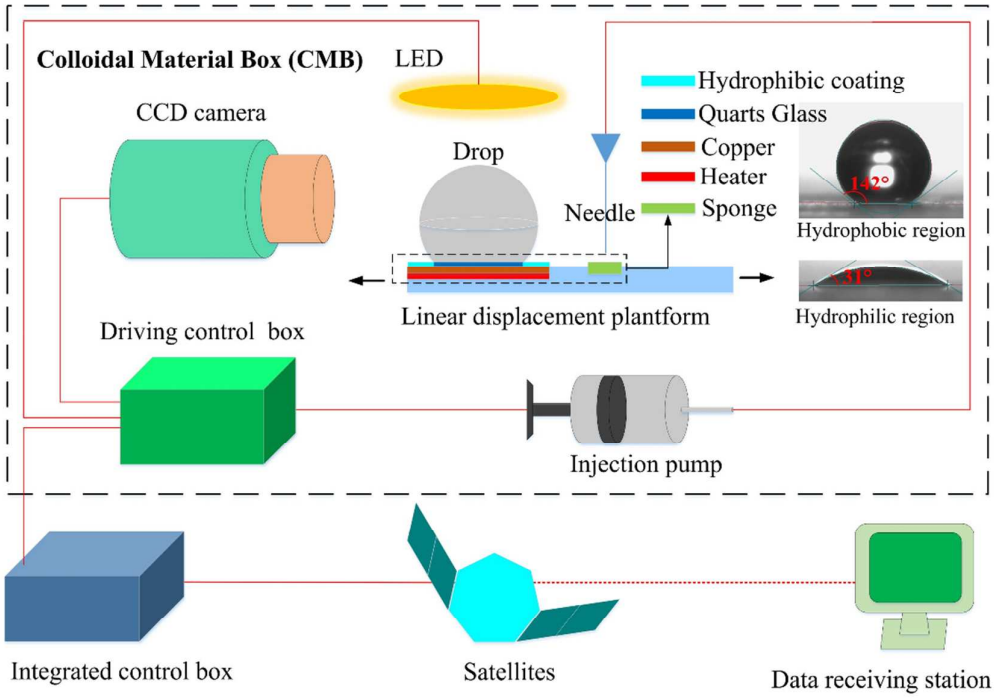

Figure 2. A schematic of the experimental setup. The inset images in the right panel are the measured contact angles of the drop on the hydrophobic and hydrophilic surface.

Patterned substrate. The patterned substrate was composed of hydrophilic and hydrophobic regions. The circular hydrophilic region was quartz glass with a diameter of 5.34 mm, which was surrounded by a hydrophobic coating (SHOS150; Shunytech). Contact angle measurements were made with ultrapure water and water-based suspension by contact angle meter (Attension Theta). The water-based suspension was aqueous colloidal solution containing polystyrene (PS) microspheres with a mean diameter of 3.03μm (Duke Scientific Corporation, 5200A). The monodisperse PS colloidal solution used in the experiment were diluted to 0.1 wt. % with high purity water. Table 2 shows advancing and receding contact angles measured on the hydrophilic and hydrophobic regions. The static contact angle of water on the hydrophilic and hydrophobic region was 31° and 142°, respectively, as shown in the left inset pictures in Figure 2. The patterned substrate could capture a large drop within the hydrophilic region and prevent it from floating away in space.

Table 1. Contact angles and hysteresis for water and water-based suspension on homogeneous surfaces

	Contact liquids					
	water			Water-based suspension		
Surfaces	θ_a (deg)	θ_r (deg)	$\Delta\theta$ (deg)	θ_a (deg)	θ_r (deg)	$\Delta\theta$ (deg)
Quartz glass	62°±2°	26°±2°	36°±4°	58°±3°	17°±1°	41°±4°
SHOS150 coating	156°±2°	134±3°	22°±5°	137°±3°	131°±3°	6°±6°

Notes：θ_a is the advancing contact angle, θ_r is the receding contact angle, and $\Delta\theta=\theta_a-\theta_r$ is the contact angle hysteresis of homogeneous surface.

Drop manipulation module. Aqueous drop would be injected from a miniature

electromagnetic pump (LPVA, Lee Co) at a rate of 11.42μL/s. The needle (062 MINSTAC, Lee Co), whose inner and outer diameter was 0.1mm and 1.3 mm, respectively, was treated as hydrophobic to repel the water from climbing. The distance between the orifice of the needle and the patterned substrate was less than 2mm,[23] so the minimum injection volume was 4.2μL (Volume of a drop with 2mm in diameter). In the injection process, the drop firstly stayed at the pinpoint of the needle. As the liquid volume increased, the drop would contact the hydrophilic surface and then rapidly spread out. Aqueous drops tended to wet the hydrophilic region but dewet the hydrophobic region, so the liquid spreading would be prevented by the hydrophobic region, and the contact radius remained the same and the height increased. By opening and closing of the valve, the drop volume could be regulated. In this way, drops with specific volume could be captured by the patterned substrate. To avoid mechanical interference from the needle, the drop would move along with the linear displacement platform (the movement speed was 0.18mm/s), which finally separated from the needle (The needle was fixed), as shown in Figure 2.

Drop evaporation module. Drop evaporation was achieved by heating the patterned substrate. The substrate, placed on the copper sheet and the heater, could be heated from the base equipped with a thermal sensor (DS18B20) for temperature acquisition. This latter was fitted with a PID temperature regulator to impose a controlled temperature. The drop was allowed to be heated from the substrate at a temperature of 40°, and evaporated in an atmosphere composed of air at a temperature of 17°±1°, and a pressure of 14 PSI. The change of the drop shape (height, contact angle and contact radius) was recorded by a CCD camera (UP610CL,UNIQ) at 1fps. The collected image data was analyzed by the Image pro 6.0 software.[23]

Driving control system. The driving control box was designed to manage the whole experimental process through controlling the run of the CMB. It could control the load operation and return the load state data to the integrated control box for packaging and downlink transfer. The collected data were transferred to the data receiving station on the ground.[23]

III. RESULTS AND DISCUSSION

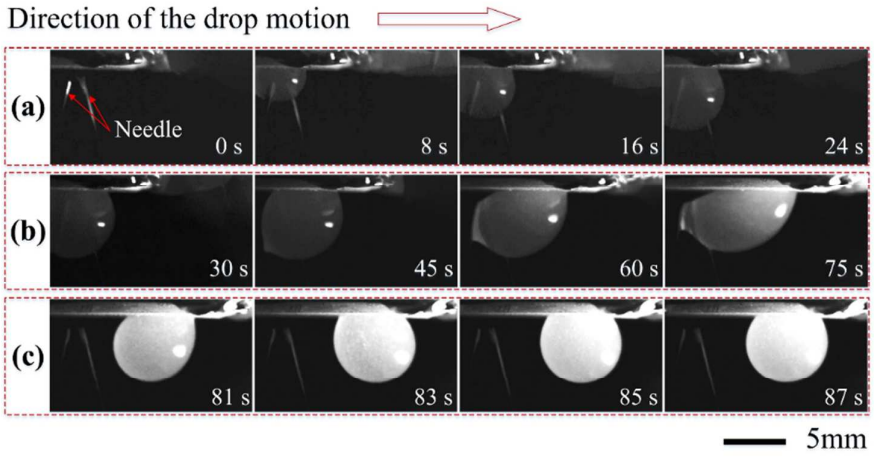

Figure 3. A large aqueous drop (160μL) was captured by the patterned substrate in microgravity

environment. (a) Drop injection from the needle. (b) Drop separation from the needle. (c) Drop oscillation and stabilization.

The patterned substrate could be used for capturing water or water-based drops in space. To demonstrate the feasibility and reliability of the drop manipulation with water-based suspension. We tested the injection, separation and oscillation of an aqueous drop in space qualitatively and got satisfactory results. As shown in Figure 3(a), an aqueous colloidal drop with volume of 160μL was injected from the needle on the hydrophilic region of the patterned substrate (video 1, Supporting Information). After the injection, the needles which was inserted into the drop should be separated from the drop itself, which could be achieved through the drop motion, as shown in Figure 3(b). Then the drop was stretched by the needles and gradually deformed to spindle shape. Although the bilateral contact angles significantly changed, the drop was still strongly attracted by the hydrophilic region of the substrate. The aqueous drop was able to bear the drag force from the needles (video 2, Supporting Information). After the drop separating from the needles, it oscillated along the drop moving direction under the action of the inertial force, as shown in Figure 3(c). After about 6 seconds, the drop restored stability and regained its original spherical cap shape (video 3, Supporting Information). The results suggested that the drop was stable enough to resist oscillation. This whole process illustrated that the patterned substrate had excellent control ability to aqueous drops in microgravity.

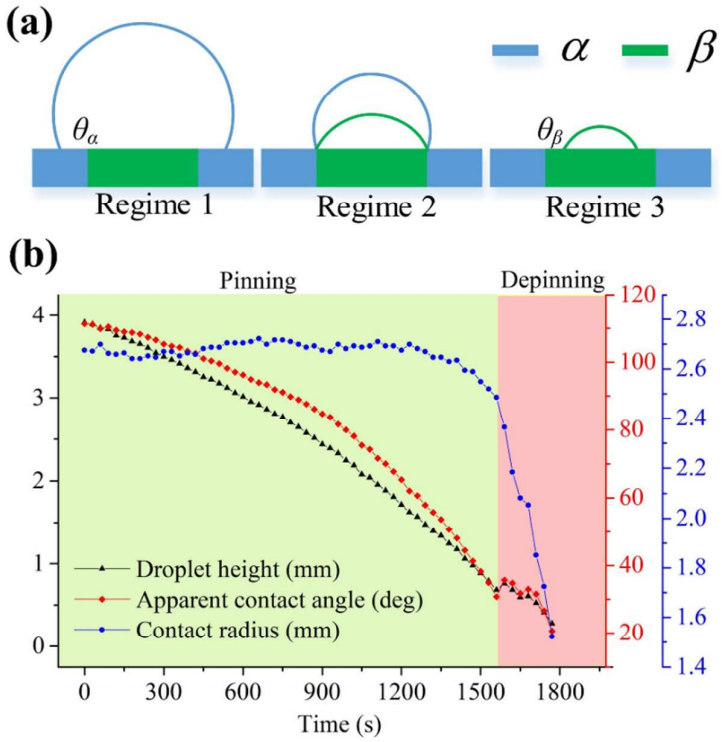

Figure 4. (a) The three wetting regimes of a drop on the ideal patterned substrate as with evaporation, where the intrinsic contact angles are θ_{α} and θ_{β} in regimes 1 and 3, respectively. The drop could be confined in regime 2. (b) Evaporation of an aqueous drop on a patterned substrate with initial volume

of 60μL under microgravity environment. The black, red, and blue line represented the drop height, the apparent contact angle, and the contact radius variation versus time t, respectively.

The capture ability of the patterned substrate was attributed to its surface wettability. Evaporation studies were useful in characterizing wetting behavior because drops with various sizes can be created to evaluate the transition criterion.[24-25] For a large drop resting on an ideal patterned substrate, with the decrease of the drop volume (V) as evaporation, three different regimes could be distinguished, as shown in Figure 4(a).[26] The intrinsic contact angles, which was determined by the chemical compositions, were θ_α and θ_β for α phase (hydrophobic region) and β phase (hydrophilic region), respectively. In regime 1 and 3, the apparent contact angle (ACA) was equal to the intrinsic contact angles. Different chemical compositions determined the wetting barrier at the interphase boundary between the hydrophilic and hydrophobic region. At this wetting barrier, the liquid surface turned from the contact angle with the better-wetting face to the contact angle with the worse-wetting face.[27] Therefore, in regime 2, the contact radius kept constant as R and the apparent contact angle (ACA) was in a closed interval $[\theta_\beta,\theta_\alpha]$. Thus, the aqueous drop of the specific volume in between $[V(R,\theta_\beta),\ V(R,\theta_\alpha)]$ could be pinned and constrained by the wetting barrier in this regime, which was responsible for the drop capturing. The super-wettable surfaces (α phase was super-hydrophobic, and the β phase was super-hydrophilic) could be chosen to achieve large drop capturing.

Figure 4(a) showed ideal homogeneous surfaces (α phase and β phase) that contact angle hysteresis (CAH) was negligible. In fact, the hysteresis could arise from any surface roughness or heterogeneity.[28] We could speculate that the range of ACA in regime 2 would be wider for real surfaces, i.e., the maximum and minimum ACA were equal to the advancing contact angle of α phase and the receding contact angle of β phase, respectively. The advancing contact angle and receding contact angle for α phase and β phase could be marked as $\theta_{\alpha a}$, $\theta_{\alpha r}$, $\theta_{\beta a}$ and $\theta_{\beta r}$ in sequence. Thus, the ACA was in a closed interval $[\theta_{\beta r}, \theta_{\alpha a}]$ in regime 2. The volume of aqueous drop that could be constrained was in between $[V(R,\theta_{\beta r}),\ V(R,\theta_{\alpha a})]$, which was larger than the ideal patterned surface. In our experiment, the quartz glass and SHOS150 coating could be considered as α phase and β phase, respectively. We had measured the contact angles and hysteresis for water and water-based suspension on these two surfaces, as shown in Table 1. The aqueous drop with ACA between 26° and 156° could be constrained by the patterned substrate. For water-based suspension drop, the ACA was in between 17° and 137°. It was realized that the range of contact angles for water-based suspension was less than the purity water, which could be attributed to the decrease the surface energy of the aqueous solution because of impurities (PS microspheres).[29]

To reveal the confinement mechanism of the substrate, evaporation experiments of water drops with different initial volumes (30μL, 40μL, 50μL, 60μL, 70μL) had been conducted under microgravity conditions. A typical drop with initial volume of 60μL was chosen to describe the wetting transition. The time evolution of the drop height, the ACA, and the contact radius, were shown in Figure 4(b). The evaporation process could be divided into two stages. In the first stage, the height and the ACA of the drop nonlinearly decreased with time, but in the meanwhile, the contact radius kept unchanged, and the drop evaporated in constant contact radius (CCR) mode. The drop evaporation spends almost all of its time in this stage, which could be characterized by the quasi-steady diffusion-driven evaporation model.[30-31] In

the last minute of evaporation, the contact line began to slip suddenly and the evaporation entered into the second stage. We noted that the ACA at the transition point (30.8°) was nearly equal to the receding contact angle of the quartz glass (26°), which fitted basically with the theoretical prediction. In the second stage, the contact radius decreased rapidly, the height and the ACA showed a broken line variation, and the drop evaporated as a skip-slip mode. What we cared about was the first stage of evaporation, which corresponded to regime 2. For water-based suspension drop, the ACA at the transition point (~17°) was less than the water drop (26°). Actually, there was no transition point for an evaporating colloidal drop, because a ring-like stain formed near the contact line,[32] which enhanced the pinning effect and made the drop evaporating as CCR mode.[33] The irregularities and unevenness at the interphase boundary between the hydrophilic and hydrophobic region of the patterned substrate was inevitable in our experiment, which would enhance the pinning effect and make the drop being confined more firmly.

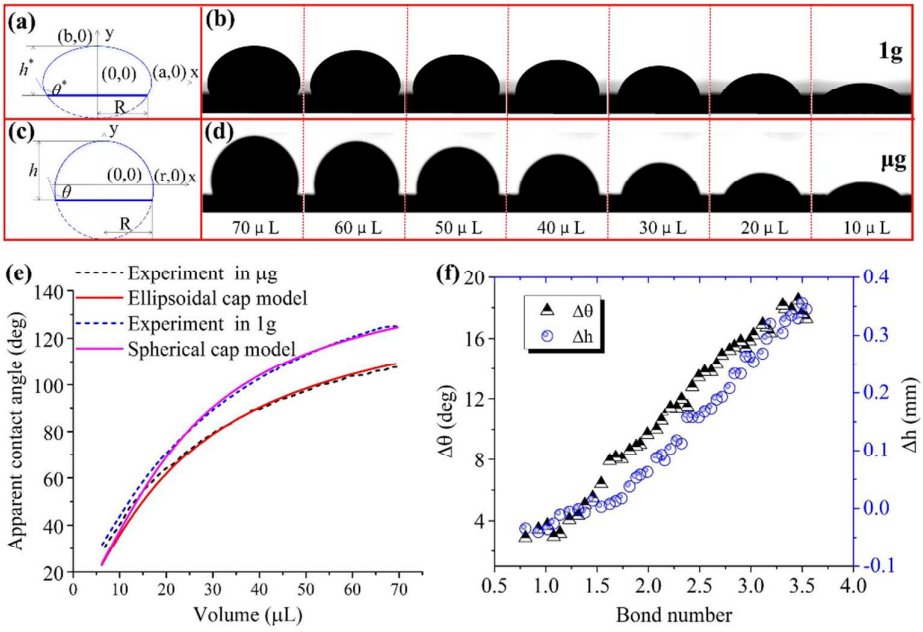

Figure 5. Geometry of an ellipsoidal cap-shaped drop model (a) and a spherical cap-shaped drop model (c) in regime 2 of the patterned substrate; Profile images of drop with different volume at normal gravity (b) and microgravity (d) conditions during the evaporation process; (e) The theoretical and experimental apparent contact angles were plotted versus volume for evaporating drops in normal gravity and microgravity (e=0.56); (f) The differences of the apparent contact angle ($\Delta\theta$) and the height (Δh) of the drop between normal gravity and microgravity were plotted versus the Bond number (Bo).

The aqueous drops in regime 2 came in different shapes in space and on the ground, which meant that the drop volumes that could be captured by the patterned substrate might be unequal under the normal gravity and microgravity. We had further studied the gravity effect on the capacity of the substrate. The drop resting on the substrate on earth could be easily distorted by gravity, its shape could be considered as an oblate ellipsoidal cap geometry [34], where h^* was the drop height, θ^* was the ACA, R was the contact radius, as shown in Figure 5(a). The eccentricity value, e, was held constant for all times. The volume of the oblate

ellipsoidal cap geometry was given by

$$V^* = \frac{\pi}{6(1-\mathrm{e}^2)}[3(1-\mathrm{e}^2)\,\mathrm{R}^2 + h^{*2}]h^* \quad (1)$$

The ACA of the drop could be expressed as

$$\theta^* = \arctan[\frac{2h^* R(1-e^2)}{(1-e^2)R^2 - h^{*2}}](1 > \mathrm{e} \geq 0) \quad (2)$$

For a drop in microgravity condition, it could be considered having the shape of a spherical cap, as shown in Figure 5(c). The drop volume V could be expressed as a function of the contact radius R, and the ACA,

$$\mathrm{V}(\mathrm{R},\theta) = \frac{\pi R^3}{3}\frac{(1-\cos\theta)^2(2+\cos\theta)}{\sin^3\theta} \quad (3)$$

The ACA could be expressed as a function of the drop height h and the contact radius R,

$$\theta = 2\arctan\frac{\mathrm{h}}{R} \quad (4)$$

Images of the drop shape with different volumes under normal gravity and microgravity were obtained through experiments, as shown in Figure 5(b) and 5(d). It was clearly seen that the difference of the drop shape increased with the liquid volume. To quantitively described the gravity effect, the ACAs were plotted versus volume in normal gravity and microgravity, as shown in Figure 5(e). The experimental results showed a well agreement with theoretical prediction, so the ellipsoidal and spherical cap model could be used to describe the drop shape in normal gravity and microgravity, respectively. When the volume was less than 10μL, the ACAs for microgravity and normal gravity were almost equal. When the volume was larger than 10μL, the ACAs increased continuously with the increased volume, and the difference of the ACAs between normal gravity and microgravity became larger. This difference was unquestionably resulted from gravity effect.

The drop shape was mainly dominated by two forces: the surface tension force, which tended to minimize the area of the surface to decrease the surface energy (producing typically a spherical shape), while the gravitational force which tended to flatten the drop. The balance of these two forces was described by the Bond number Bo, $Bo=(\rho_L-\rho_V)gL^2/\sigma$, where, ρ_L was the density of the liquid, ρ_V was the density of the vapor, L was the characteristic length, g was the gravitational acceleration, and σ was the liquid-vapor surface tension.[35] It was critical to choose the characteristic length. Here, the drop was considered to be equivalent to the spherical drop with the same volume, and we chose the diameter of this spherical drop as the characteristic length, thus the Bond number (Bo) of the drops with different equivalent volumes (V_e) in normal gravity could be calculated. The differences of the ACA ($\Delta\theta=\theta^*-\theta$) and the height ($\Delta h=h-h^*$) of the drop between normal gravity and microgravity were plotted versus the Bond number, as shown in Figure 5(f). $\Delta\theta$ and Δh could be used to judge the shape deviation of the drop in normal gravity from an ideal spherical cap drop in microgravity. When the Bo<1 (V_e<10.3μL), $\Delta\theta$ and Δh was close to zero, which meant that the drop shape could be hardly affected by gravity. When the Bo=1 (V_e=10.3μL), the characteristic length L= 2.7mm (the capillary length), the equivalent volume

of the drop was 10.3μL, which coincided with the experimental results (10μL), as shown in Figure 5(e). When the Bo>1 (V_e=10.3μL), $\Delta\theta$ and Δh increased as with increasing of the Bond number, so the flattening effect of the drop resulting from gravity was more pronounced for higher values of the Bond number. It indicated that the ACA could be easier to reach to the advancing contact angle of the hydrophobic region for drops in normal gravity, so this patterned substrate could confine drops with greater volume in space than on earth. The patterned substrate used in our experiment could confine a drop with extreme volume of only 148μL in normal gravity but 329μL in microgravity. Therefore, the gravity effect significantly influenced the confinement capacity of the patterned substrate, the bigger the drop volume, the larger the gravity effect on its confinement capacity.

IV. CONCLUSIONS

In summary, we had successfully conducted drop manipulation experiments in space. The drop could be captured by a patterned substrate, which was composed of a circular hydrophilic matrix surrounded by hydrophobic coating. Through the test of injection, separation and oscillation of a colloidal drop, it could be shown that this patterned substrate had excellent ability of capturing aqueous drops in space. The confinement mechanism of the substrate was investigated by monitoring the behaviors of evaporating drops, which showed that drops with specific volumes could be pinned and attracted at a given area on the substrate. The gravity effect on the confinement capacity was further investigated theoretically and experimentally under the conditions of both normal gravity and microgravity. It indicated the confined drop could be considered as a spherical and ellipsoidal cap model in microgravity and normal gravity, respectively, and the substrate could confine aqueous drops with larger volume under microgravity than in normal gravity. With advantages of simple operation, strong capacity to capturing large drops in space, this technique showed promising prospects in fluid management, bio-sensing, and pharmacy in microgravity conditions in the future.

ASSOCIATED CONTENT

Supporting Information

Drop injection from the needle in space (Video S1).
Drop separation from the needle in space (Video S2).
Drop oscillation and stabilization in space (Video S3).

AUTHOR INFORMATION

Corresponding Author

E-mail: *landing@imech.ac.cn; †yurenwang@imech.ac.cn.

ACKNOWLEDGEMENTS

We gratefully acknowledge financial support from the National Natural Science Foundation of China (Grant Nos U1738118 and 11472275), the Strategic Priority Research Program on Space Science, Chinese Academy of Sciences (Grant Nos XDA04020202 and XDA04020406), and the Strategic Priority Research Program of the Chinese Academy of Sciences (Grant No. XDB22040301).

REFERENCES

1. Kabov, O. A.; Bartashevich, M.; Cheverda, V., Rivulet Flows in Microchannels and Minichannels. *International Journal of Emerging Multidisciplinary Fluid Sciences* **2010,** *2*.
2. Conrath, M.; Canfield, P.; Bronowicki, P.; Dreyer, M. E.; Weislogel, M. M.; Grah, A., Capillary channel flow experiments aboard the International Space Station. *Physical review E* **2013,** *88* (6), 063009.
3. Bostwick, J.; Steen, P., Stability of constrained capillary surfaces. *Annual Review of Fluid Mechanics* **2015,** *47*, 539-568.
4. Antar, B. N.; Ethridge, E. C.; Maxwell, D., Viscosity measurement using drop coalescence in microgravity. *Microgravity Science and Technology* **2003,** *14* (1), 9-19.
5. Savino, R.; Nota, F.; Fico, S., Wetting and coalescence prevention of drops in a liquid matrix. Ground and parabolic flight results. *Microgravity Science and Technology* **2003,** *14* (3), 3-12.
6. Brutin, D.; Zhu, Z.; Rahli, O.; Xie, J.; Liu, Q.; Tadrist, L., Sessile drop in microgravity: creation, contact angle and interface. *Microgravity Science and Technology* **2009,** *21* (1), 67-76.
7. Herminghaus, S.; Brinkmann, M.; Seemann, R., Wetting and dewetting of complex surface geometries. *Annu. Rev. Mater. Res.* **2008,** *38*, 101-121.
8. Nakajima, A., Design of hydrophobic surfaces for liquid droplet control. *NPG Asia Materials* **2011,** *3*, 49.
9. Zhao, X. D.; Fan, H. M.; Liu, X. Y.; Pan, H.; Xu, H. Y., Pattern-dependent tunable adhesion of superhydrophobic MnO2 nanostructured film. *Langmuir* **2011,** *27* (7), 3224-3228.
10. Liu, K.; Cao, M.; Fujishima, A.; Jiang, L., Bio-inspired titanium dioxide materials with special wettability and their applications. *Chemical reviews* **2014,** *114* (19), 10044-10094.
11. Bormashenko, E., Progress in understanding wetting transitions on rough surfaces. *Advances in colloid and interface science* **2015,** *222*, 92-103.
12. Lai, Y.; Huang, J.; Cui, Z.; Ge, M.; Zhang, K. Q.; Chen, Z.; Chi, L., Recent Advances in TiO2□ Based Nanostructured Surfaces with Controllable Wettability and Adhesion. *Small* **2016,** *12* (16), 2203-2224.
13. Lai, Y.; Pan, F.; Xu, C.; Fuchs, H.; Chi, L., In Situ Surface□Modification□Induced Superhydrophobic Patterns with Reversible Wettability and Adhesion. *Advanced Materials* **2013,** *25* (12), 1682-1686.
14. Tenjimbayashi, M.; Higashi, M.; Yamazaki, T.; Takenaka, I.; Matsubayashi, T.; Moriya, T.; Komine, M.; Yoshikawa, R.; Manabe, K.; Shiratori, S., Droplet Motion Control on Dynamically Hydrophobic Patterned Surfaces as Multifunctional Liquid Manipulators. *ACS Applied Materials & Interfaces* **2017,** *9* (12), 10371-10377.
15. Dong, T.; McCarthy, T. J., Superhydrophobic, Low-Hysteresis Patterning Chemistry for Water-Drop Manipulation. *ACS applied materials & interfaces* **2017,** *9* (47), 41126-41130.
16. Draper, M. C.; Crick, C. R.; Orlickaite, V.; Turek, V. A.; Parkin, I. P.; Edel, J. B., Superhydrophobic surfaces as an on-chip microfluidic toolkit for total droplet control. *Analytical chemistry* **2013,** *85* (11), 5405-5410.
17. Zhang, S.; Huang, J.; Tang, Y.; Li, S.; Ge, M.; Chen, Z.; Zhang, K.; Lai, Y., Understanding the Role of Dynamic Wettability for Condensate Microdrop Self□Propelling Based on Designed Superhydrophobic TiO2 Nanostructures. *small* **2017,** *13* (4).
18. Wu, L.; Dong, Z.; Li, F.; Song, Y., Designing Laplace Pressure Pattern for Microdroplet

Manipulation. *Langmuir* **2018,** *34* (2), 639-645.

19. Stange, M.; Dreyer, M. E.; Rath, H. J., Capillary driven flow in circular cylindrical tubes. *Physics of fluids* **2003,** *15* (9), 2587-2601.

20. Dreyer, M.; Delgado, A.; Path, H.-J., Capillary rise of liquid between parallel plates under microgravity. *Journal of Colloid and interface science* **1994,** *163* (1), 158-168.

21. Wang, C.-X.; Xu, S.-H.; Sun, Z.-W.; Hu, W.-R., A study of the influence of initial liquid volume on the capillary flow in an interior corner under microgravity. *International Journal of Heat and Mass Transfer* **2010,** *53* (9), 1801-1807.

22. Hu, W.; Zhao, J.; Long, M.; Zhang, X.; Liu, Q.; Hou, M.; Kang, Q.; Wang, Y.; Xu, S.; Kong, W., Space program SJ-10 of microgravity research. *Microgravity Science and Technology* **2014,** *26* (3), 159-169.

23. Li, W.; Lan, D.; Sun, Z.; Geng, B.; Wang, X.; Tian, W.; Zhai, G.; Wang, Y., Colloidal Material Box: In-situ Observations of Colloidal Self-Assembly and Liquid Crystal Phase Transitions in Microgravity. *Microgravity Science and Technology* **2016,** *28* (2), 179-188.

24. Tsai, P.; Lammertink, R. G.; Wessling, M.; Lohse, D., Evaporation-triggered wetting transition for water droplets upon hydrophobic microstructures. *Physical review letters* **2010,** *104* (11), 116102.

25. Jung, Y. C.; Bhushan, B., Wetting transition of water droplets on superhydrophobic patterned surfaces. *Scripta Materialia* **2007,** *57* (12), 1057-1060.

26. Lenz, P.; Lipowsky, R., Morphological transitions of wetting layers on structured surfaces. *Physical review letters* **1998,** *80* (9), 1920.

27. Langbein, D., Canthotaxis/wetting barriers/pinning lines. *Capillary Surfaces* **2002**, 149-177.

28. Extrand, C., Contact angles and hysteresis on surfaces with chemically heterogeneous islands. *Langmuir* **2003,** *19* (9), 3793-3796.

29. Park, J. K.; Ryu, J.; Koo, B. C.; Lee, S.; Kang, K. H., How the change of contact angle occurs for an evaporating droplet: effect of impurity and attached water films. *Soft Matter* **2012,** *8* (47), 11889-11896.

30. Girard, F.; Antoni, M.; Faure, S.; Steinchen, A., Influence of heating temperature and relative humidity in the evaporation of pinned droplets. *Colloids and Surfaces A: Physicochemical and Engineering Aspects* **2008,** *323* (1), 36-49.

31. Hu, H.; Larson, R. G., Evaporation of a sessile droplet on a substrate. *The Journal of Physical Chemistry B* **2002,** *106* (6), 1334-1344.

32. Deegan, R. D.; Bakajin, O.; Dupont, T. F.; Huber, G., Capillary flow as the cause of ring stains from dried liquid drops. *Nature* **1997,** *389* (6653), 827.

33. Weon, B. M.; Je, J. H., Self-pinning by colloids confined at a contact line. *Physical review letters* **2013,** *110* (2), 028303.

34. Erbil, H. Y.; Meric, R. A., Evaporation of sessile drops on polymer surfaces: Ellipsoidal cap geometry. *The Journal of Physical Chemistry B* **1997,** *101* (35), 6867-6873.

35. Diana, A.; Castillo, M.; Brutin, D.; Steinberg, T., Sessile drop wettability in normal and reduced gravity. *Microgravity Science and Technology* **2012,** *24* (3), 195-202.

Table of Contents

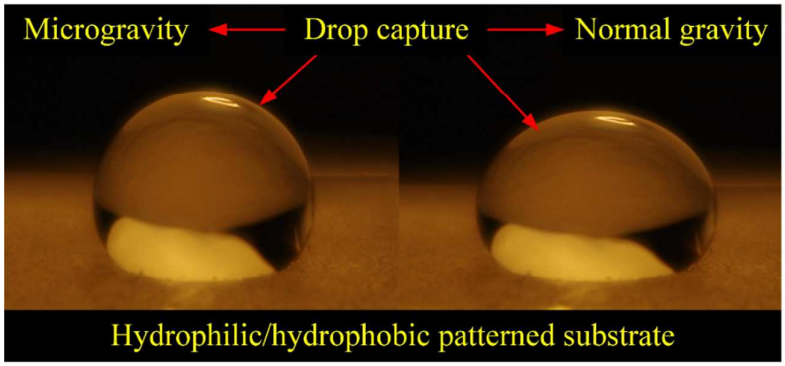
Microgravity
Drop capture
Normal gravity
Hydrophilic/hydrophobic patterned substrate

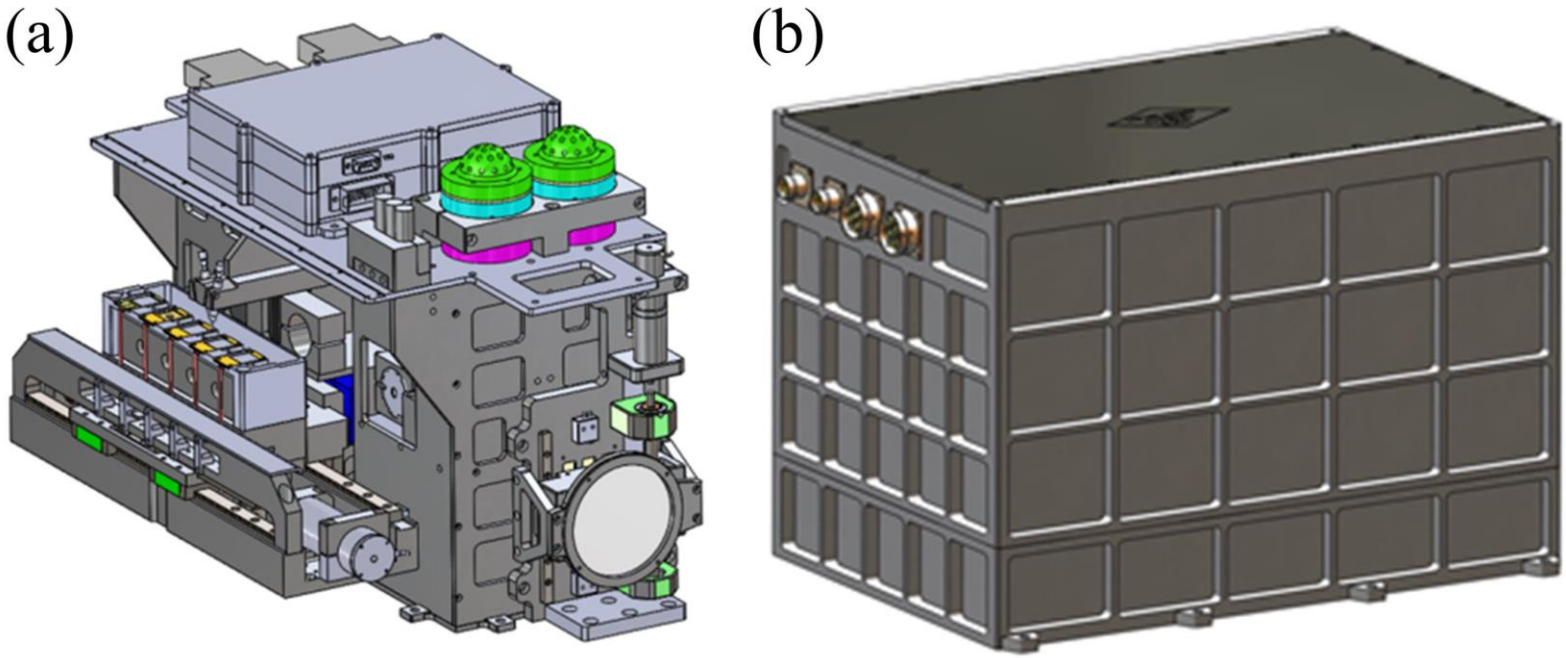
(a)
(b)

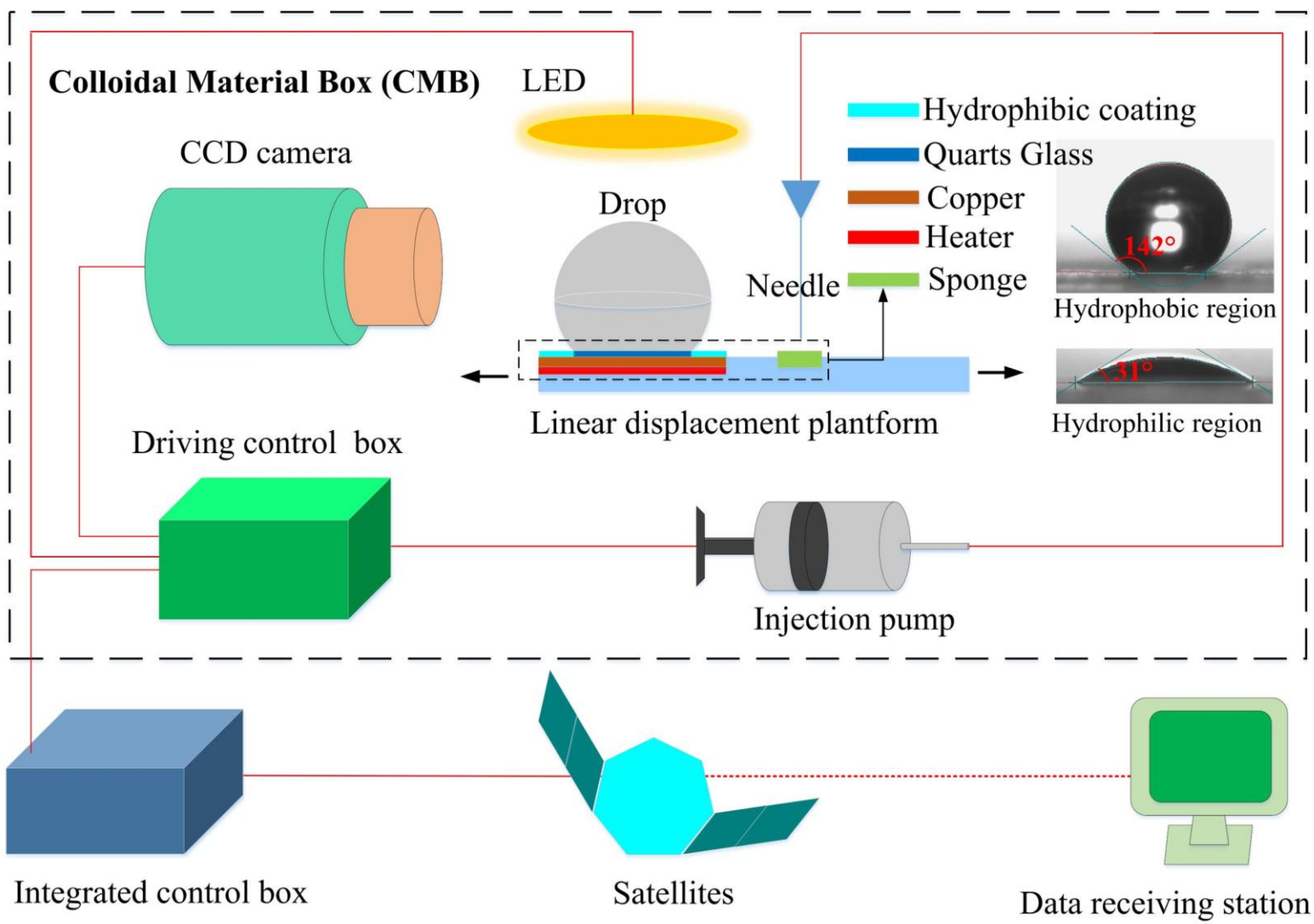
Colloidal Material Box (CMB)
LED
CCD camera
Drop
Needle
Hydrophibic coating
Quarts Glass
Copper
Heater
Sponge
142°
Hydrophobic region
31°
Hydrophilic region
Linear displacement plantform
Driving control box
Injection pump
Integrated control box
Satellites
Data receiving station

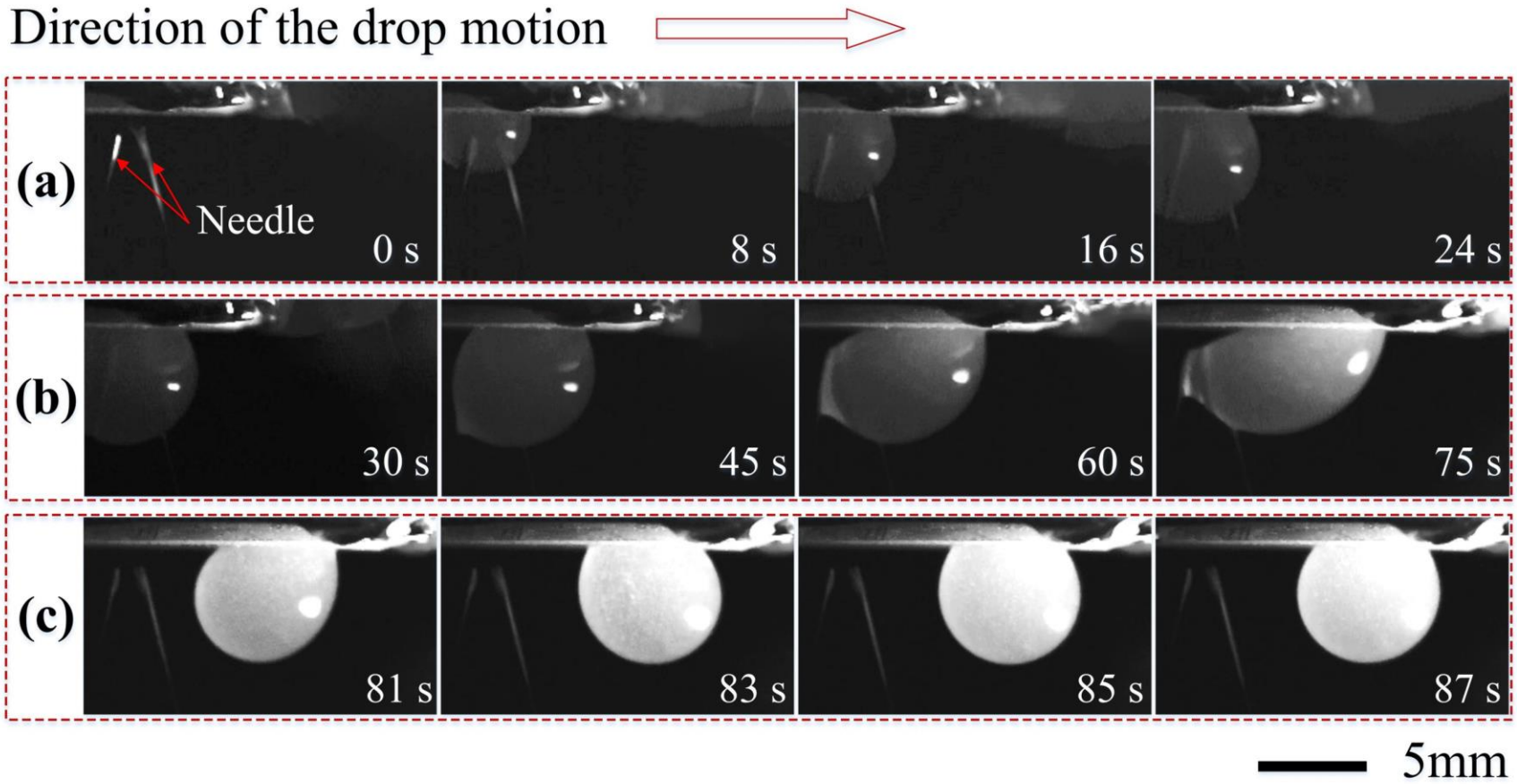
Direction of the drop motion
(a)
Needle
0 s
8 s
16 s
24 s
(b)
30 s
45 s
60 s
75 s
(c)
81 s
83 s
85 s
87 s
5mm

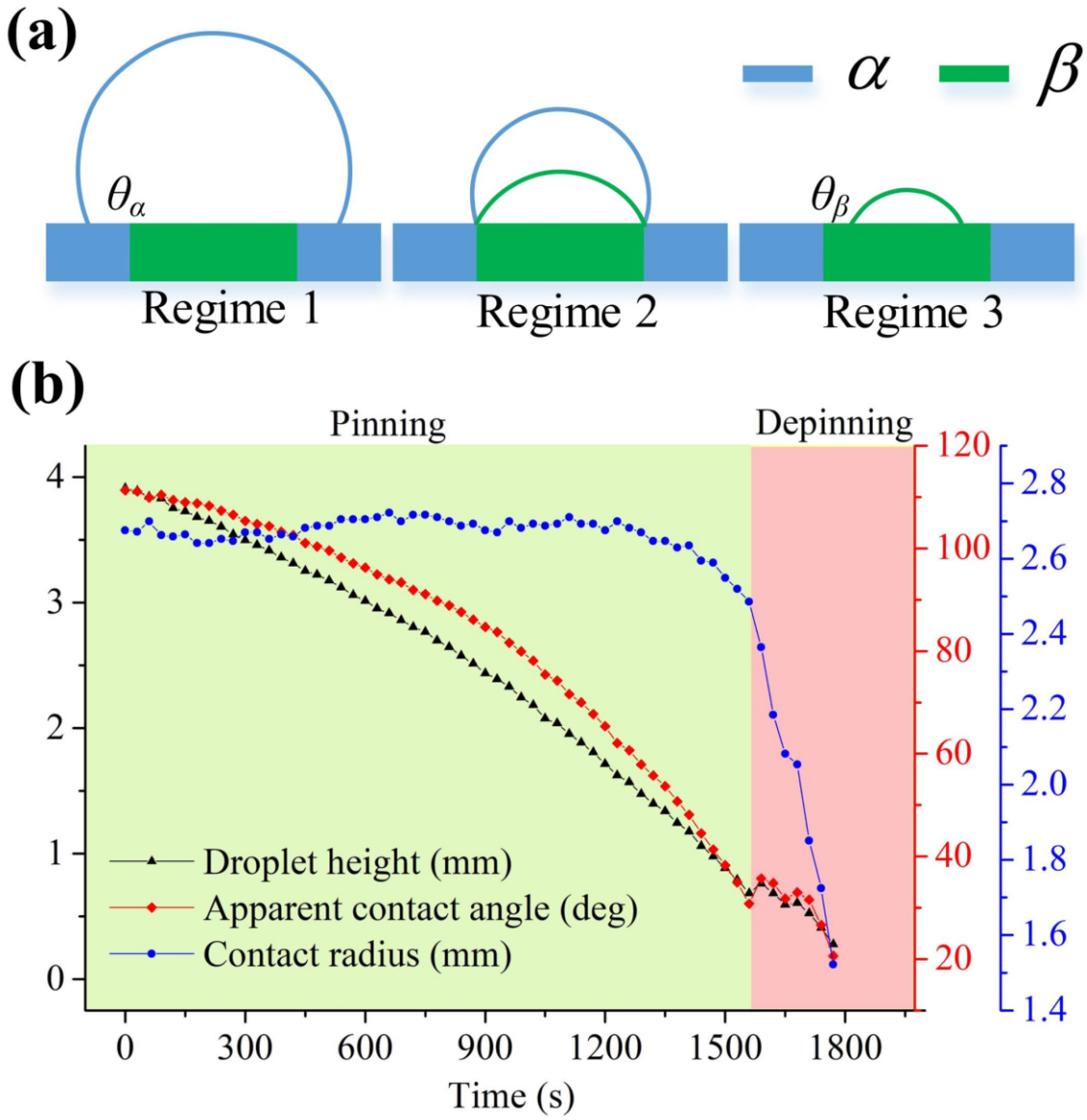
(a)
α
β
θα
θβ
Regime 1
Regime 2
Regime 3
(b)
Pinning
Depinning
Droplet height (mm)
Apparent contact angle (deg)
Contact radius (mm)
Time (s)
0
300
600
900
1200
1500
1800
0
1
2
3
4
20
40
60
80
100
120
1.4
1.6
1.8
2.0
2.2
2.4
2.6
2.8

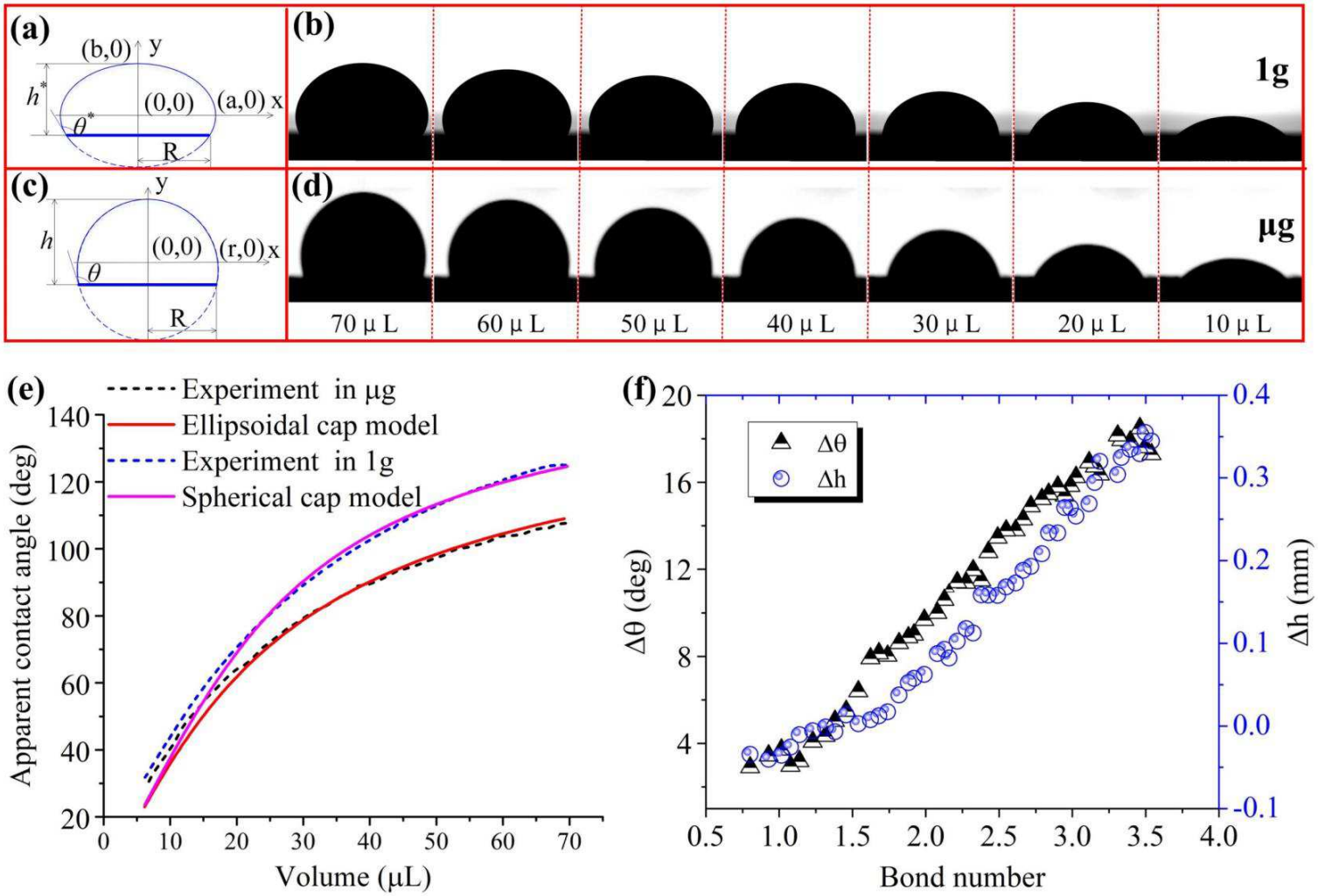
(a)
(b,0)
y
h*
(0,0)
(a,0) x
θ*
R
(b)
1g
(c)
y
h
(0,0)
(r,0) x
θ
R
(d)
μg
70 μ L
60 μ L
50 μ L
40 μ L
30 μ L
20 μ L
10 μ L
(e)
Experiment in μg
Ellipsoidal cap model
Experiment in 1g
Spherical cap model
Apparent contact angle (deg)
Volume (μL)
(f)
Δθ
Δh
Δθ (deg)
Δh (mm)
Bond number

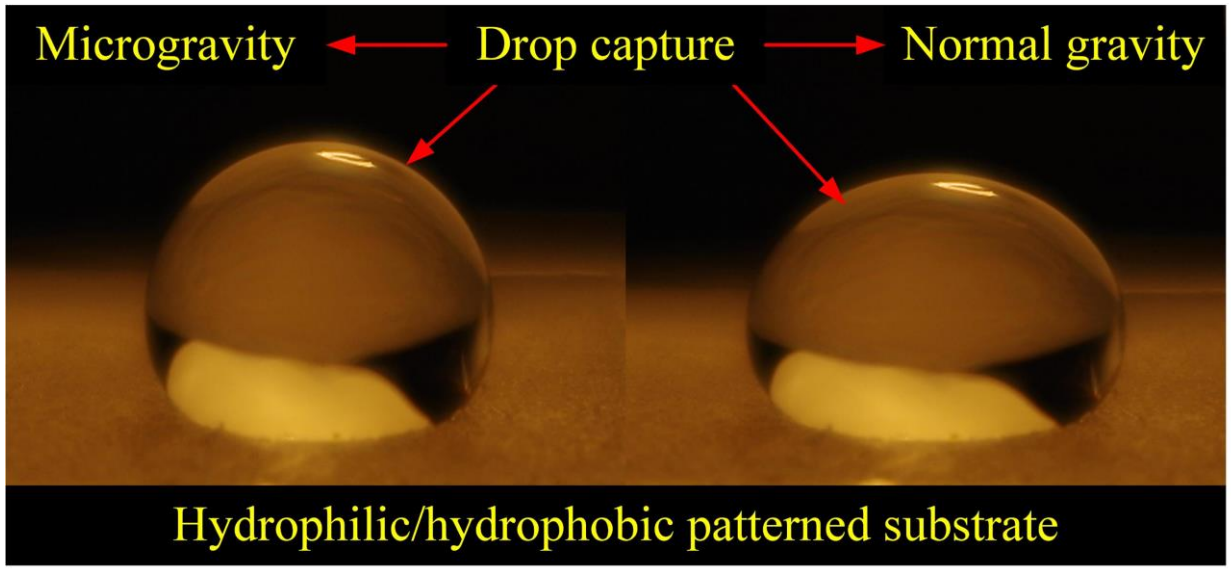
Microgravity
Drop capture
Normal gravity
Hydrophilic/hydrophobic patterned substrate